IJRCS

International Journal of Robotics and Control Systems
Vol. 3, No. 3, 2023, pp. 433-448
ISSN 2775-2658
http://pubs2.ascee.org/index.php/ijrcs

ASCEE

Magnetometer-Only Kalman Filter Based Algorithms for High Accuracy Spacecraft Attitude Estimation (A Comparative Analysis)

Tamer Mekky Ahmed Habib [a,1,*]

[a] National Authority for Remote Sensing and Space Sciences, 23, Josef Tito St., Nozha El-Gedida, Cairo and 1564, Egypt
[1] tamermekky@hotmail.com
* Corresponding Author

ARTICLE INFO

Article history
Received April 03, 2023
Revised May 13, 2023
Accepted July 01, 2023

Keywords
Magnetometer Only;
Kalman Filter;
High Accuracy

ABSTRACT

Kalman Filter (KF) based algorithms are the most frequently employed attitude estimation algorithms. Typically, a fully observable system necessitates the use of two distinct sensor types. Therefore, relying on a single sensor, such as a magnetometer, for spacecraft attitude estimation is deemed to be a challenge. The present investigation centers on utilizing magnetometers as the exclusive sensor. Several KF based estimation algorithms have been designed and evaluated to give the designer of spacecraft Attitude and Orbit Control System (AOCS) the choice of a suitable algorithm for his mission based on quantitative measures. These algorithms are capable of effectively addressing nonlinearity in both process and measurement models. The algorithms under examination encompass the Extended Kalman Filter (EKF), Sequential Extended Kalman Filter (SEKF), Pseudo Linear Kalman Filter (PSELIKA), Unscented Kalman Filter (USKF), and Derivative Free Extended Kalman Filter (DFEKF). The comparison of the distinct algorithms hinges on key performance metrics, such as estimation error for each axis, computation time, and convergence rate. The resulting algorithms provide numerous benefits, such as diverse levels of high estimation accuracy (with estimation errors ranging from 0.014° to 0.14°), varying computational demands (execution time ranges from 0.0536s to 0.0584s), and the capability to converge despite large initial attitude estimation errors (which reached 170°). These properties render the algorithms appropriate for utilization by spacecraft designers in all operational modes, supplying high-precision attitude estimations better than (0.5°) despite high magnetometer noise levels, which reached (200 nT).

1. Introduction

The primary job of spacecraft Attitude and Orbit Control System (AOCS) is to measure, estimate, and control spacecraft attitude angles in addition to spacecraft orbit. In numerous instances, it is not possible to measure spacecraft attitude angles (which need to be controlled) directly via sensors. As a result, an attitude estimation algorithm is necessary to establish a connection between sensor measurements and the spacecraft's intended attitude angles, while simultaneously minimizing the impact of measurement noise and process disturbance. Kalman Filter (KF) and its derivatives are the

most frequently employed attitude estimation algorithms for such purposes. In 1960, Kalman developed his numerical filter to estimate system states recursively based on measurements of sensors and named his filter as KF [1]. The filter estimated the desired system states optimally (in a least squares sense) in the presence of random zero-mean white Gaussian sensor noise, and disturbance effects. The filter was based on numerical solution rather than an exact closed form solution. Since then, computers continued to evolve and KF began to attract research interest because of its suitability for computer-based control systems. A Major drawback of the KF was its ability to handle only linear systems, and linear measurement processes. Thus, an extension was made for the KF to enable handling of nonlinear situations and named as Extended Kalman Filter (EKF). Several algorithms now exist in the literature to handle nonlinearities based on KF. These algorithms include, Sequential Extended Kalman Filter (SEKF), Pseudo Linear Kalman Filter (PSELIKA), Unscented Kalman Filter (USKF), and Derivative Free Extended Kalman Filter (DFEKF). SEKF is based on sequential formulation of the Extended Kalman Filter [2][3]. In this approach, the measurements are fed into filter in a scalar form rather than a vector form. PSELIKA reshapes the non-linear plant and process equations into a form similar to linear systems while keeping the nonlinearities. USKF propagates (2N+1) sigma points (where N is the number of system states to be estimated) ahead of time in order to avoid the approximations used by EKF to compute the state transition, and measurement matrices. The DFEKF belongs to the same family of USKF but it propagates only (N+1) sigma points instead of (2N+1). A comprehensive review for KF, EKF, PSELIKA, USKF, and DFEKF could be found in [4].

Typically, a fully observable system necessitates the use of two distinct sensor types. Therefore, relying on a single sensor, such as a magnetometer, for spacecraft attitude estimation is deemed to be a challenge. Spacecraft attitude estimation involves measuring physical quantities in the spacecraft's body axes. Magnetometers are widely used as the primary sensors for this purpose. Nearly all spacecraft AOCSs include a three-axis magnetometer to measure the three components of the earth's magnetic in the x, y, and z directions of the body axes. Magnetometers have several advantages, including a long lifespan and increased reliability due to the absence of moving parts, as well as a relatively low cost compared to other AOCS sensors. These factors contribute to the widespread use of magnetometers as spacecraft attitude sensors. Incorporating other spacecraft attitude sensors with magnetometers can present some challenges, as seen in single frame attitude determination methods [5]. One issue is the lack of sun sensor measurements during eclipse periods as the spacecraft orbits around the earth. Additionally, the accumulation of errors can limit the ability of gyros to function over a long period of time. Star sensors, while able to provide highly accurate attitude estimates, are limited in their use due to the high energy consumption required, which can put a strain on the already limited power supply available to the spacecraft. To overcome all of the challenges associated with using other sensors, the only solution is to use a magnetometer as a sole attitude sensor.

Numerous studies and research papers have explored the use of magnetometers for spacecraft attitude estimation. For instance, in [6], a Three-Axis Magnetometer (TAM) was utilized to determine both the orbit and attitude of the spacecraft. The algorithms developed were limited to only being able to handle an initial attitude estimation error of 16^{o}. In another study [7], spacecraft attitude was estimated solely using magnetometer measurements. The algorithms developed were capable of handling an initial attitude estimation error of 45^{o}. In reference [4], several approaches for estimating spacecraft attitude are presented. According to [8], some attitude determination techniques are not frequently used due to their high computational demands, which can limit or even prevent their use in real-time on board the spacecraft. This is particularly relevant because many commercially operated spacecrafts use processors that are 15 or even 20 years old [9]. The reason for this is that certifying a particular processor to work in the space environment takes extensive periods of time and requires it to be part of multiple missions. As a result, algorithms like the ones found in [10] would not be easily adaptable to a processor that's over 20 years old.

According to [11], various techniques have been studied for figuring out the orientation of spacecraft without gyros, using only a sun sensor and a magnetometer. Ref. [12] goes on to discuss algorithms specifically designed to estimate the attitude of a spacecraft based on these two

instruments. However, it's worth noting that these algorithms have a limitation - they can only handle a maximum initial error of 60º. In [13], the use of the (TAM) was explored for attitude estimation. Although the method was used, the results showed a steady state error of 14º in the yaw axis, which is considered a relatively large discrepancy. Ref. [14] takes a different approach, focusing on the use of a magnetometer for determining the orientation of a spacecraft in a single axis. Therefore, it was impossible to calculate the three-axis attitude estimates. In [15], magnetometer provided linear estimates of the spacecraft's attitude with a constant error of 3º, which is considered a large number. In [16], Magnetometer measurements are used along with the Unscented Kalman Filter (USKF). Errors of the attitude estimates were improved to 0.3º. It is widely known that the USKF requires a lot more computation compared to the Extended Kalman Filter (EKF) due to the need to process multiple sigma points.

Using a Standard KF or EKF may not be the optimal choice because they include matrix inversion operations which are computationally expensive for the spacecraft's on-board computer (OBC). Thus, they are not ideal from a computational cost perspective. Ref. [2] Developed an estimator for spacecraft attitude estimation based solely on magnetometer measurements via Sequential Extended Kalman Filter (SEKF) to avoid matrix inversion operations. The developed algorithm is capable of providing high accuracy attitude estimates even if two of the three channels of the magnetometer are not functioning. In addition, the developed algorithm could deal effectively with high initial attitude estimation error and still able to converge. A third advantage is the faster execution time onboard the spacecraft processor. Ref. [17] assessed different algorithms for spacecraft attitude estimation and determination based on measurements of a magnetometer augmented with gyros via EKF.

Ref. [18] presented a comprehensive review on state-of-the-art algorithms utilized for spacecraft Guidance, Navigation, and Control (GNC) purposes. These algorithms included Artificial Intelligence (AI) techniques. Some AI algorithms require training data set such as those given in [19]- [26]. In this case, the only means to provide large enough training data set is through simulation. In [19], a spacecraft attitude control algorithm is developed based on Adaptive Neuro-Fuzzy Inference System (ANFIS). In [20], a Neural Networks (NN) based algorithm is developed for the same problem. In [21], a spacecraft orbit control algorithm is based on NN. In [22], spacecraft attitude determination and estimation algorithm are achieved via NN. In [23], an EKF for spacecraft orbit estimation is totally replaced via NN. In [24], spacecraft attitude determination and estimation algorithm are achieved via ANFIS. In [25], a model for spacecraft orbit is obtained via NN. Simultaneous estimation for spacecraft orbital and attitude states is obtained through NN as contributed in [26]. The current research article could be utilized to provide training data set in order to train AI based algorithms for spacecraft GNC purposes. The developed algorithms in the current research article could be easily combined with Refs [19]-[26] to provide an integrated solution for the spacecraft AOCS.

The main objective of the current research article is to provide the designer of the AOCS with various choices of spacecraft attitude estimation algorithms, and compare these choices with qualitative measures to select the best fitting for a certain spacecraft mission. The current research article offers several contributions. The first contribution is developing various spacecraft attitude estimation algorithms utilizing only magnetometer readings through the use of several KF based algorithms. The second contribution is assessing these algorithms (which include EKF, SEKF, PSELIKA, USKF, and DFEKF) using important performance metrics such as attitude estimation error in each axis, algorithm processing speed, and rate of convergence. The newly developed algorithms are compared to verified EKF, and SEKF algorithms which were used to estimate the attitude of the Egyptian Satellite EGYPTSAT-1 in [2][17]. The third contribution is the ability of all of the developed algorithms to provide high accuracy estimates of spacecraft attitude angles based solely on magnetometer measurements, which was not possible before. The newly developed algorithms boast several benefits including:

1- The capability to handle extremely nonlinear situations.

2- Offering a solution for the spacecraft attitude estimation problem that does not involve singularities.

3- Capability of the developed algorithms to handle a single type of measurements, such as the measurement of the earth's magnetic field.
4- Supplying accurate estimates of a spacecraft's attitude whenever required.
5- Ability to converge even with a substantial initial error in attitude estimation.
6- Ability to provide complete three-dimensional attitude information.

This study is organized in the following manner: In Section 2, a method of solution is proposed. Models of nonlinear spacecraft motion are presented. Necessary estimation algorithms are also outlined in this section. Section 3 includes the simulation results and discussions. Finally, the conclusions are summarized in Section 4.

2. Method

2.1. Nonlinear Spacecraft Motion Models

The translational motion model of the spacecraft is described using Cowell's formulation. It is expressed as Equation (1).

$$\ddot{R}_I = -\frac{\mu_E}{\|R_I\|^3} R_I + a_a \tag{1}$$

Where, the spacecraft position vector is defined with respect to the Earth Centered Inertial (ECI) coordinate system and represented by R_I. The gravitational constant of the earth is represented by μ_E, and the perturbing acceleration caused by the Earth's asphericity is represented by a_a (with its calculation details given in [18]).

The Kinematic equations for the spacecraft's attitude motion are described by the following relationship in Equation (2).

$$\dot{Q}_{I\to B} = \frac{1}{2}\Xi Q_{I\to B} \tag{2}$$

Where, $Q_{I\to B} = [q_1 \quad q_2 \quad q_2 \quad q_4]^T$, is a quaternion vector having real part, q_4, which transforms a vector from the ECI to Body Coordinate System (BCS). The Matrix, Ξ, is represented by the following relationship in Equation (3).

$$\Xi = \begin{bmatrix} 0 & \omega_z & -\omega_y & \omega_x \\ -\omega_z & 0 & \omega_x & \omega_y \\ \omega_y & -\omega_x & 0 & \omega_z \\ -\omega_x & -\omega_y & -\omega_z & 0 \end{bmatrix} \tag{3}$$

Where, $\omega = [\omega_x \quad \omega_y \quad \omega_z]^T$ is the vector representing the spacecraft's angular velocities in the inertial frame. The dynamic motion of the spacecraft's rotation is represented by the following relationship in Equation (4).

$$\dot{\omega} = J^{-1}[(J\omega + H_\omega)\times]\omega + J^{-1}\left(T_g + T_a + T_r + T_s\right) + w_k \tag{4}$$

Where T_g, T_a, T_r, T_s, are the torques resulting from gravity gradient, aerodynamics, residual magnetism, and solar pressure, respectively, and H_ω represents the angular momentum vector of any moving parts, Additionally, w_k is a zero-mean white Gaussian noise linked to process noise. Information on calculating the disturbance torques can be found in [17]. The cross product equivalent matrix $[\beta\times]$ for the vector $\beta = [\beta_x \quad \beta_y \quad \beta_z]^T$ is represented as Equation (5).

$$[\beta\times] = \begin{bmatrix} 0 & -\beta_z & \beta_y \\ \beta_z & 0 & -\beta_x \\ -\beta_y & \beta_x & 0 \end{bmatrix} \tag{5}$$

The spacecraft's inertia matrix, J, is expressed as Equation (6).

$$J = \begin{bmatrix} J_x & -J_{xy} & -J_{xz} \\ -J_{xy} & J_y & -J_{yz} \\ -J_{xz} & -J_{yz} & J_z \end{bmatrix} \quad (6)$$

The choice of the spacecraft attitude motion state vector is crucial, as it is a key factor in any attitude estimation algorithm. The state vector representing the spacecraft attitude motion has been selected as Equation (7).

$$X = [q_1 \quad q_2 \quad q_3 \quad q_4 \quad \omega_x \quad \omega_y \quad \omega_z] \quad (7)$$

The state vector expressed in Equation (7) has the benefit of being able to depict any attitude maneuver without encountering singularities, which prevents the entire developed algorithm from collapsing. Furthermore, selecting the orbital state vector as the inertial position and inertial velocity, as shown in (1), also avoids singularity issues in certain types of orbits for the entire simulation.

2.2. Spacecraft attitude estimation algorithms

The goal of any spacecraft attitude estimation algorithm is to accurately determine the orientation of the spacecraft based on noisy measurements with the existence of random disturbances. Singular Value Decomposition (SVD) based algorithms are not a popular choice because they can be computationally intensive [5] for the limited computational resources available on a spacecraft. KF based algorithms are more commonly used because of several reasons:

1- Avoiding the solution of an eigenvalue problem in real-time situations which is computationally intensive.

2- A real-time algorithm can be developed using these algorithms.

3- Ability to handle non-linear situations.

4- Ability to handle large initial attitude estimation errors which could be encountered during spacecraft flight in its orbit.

KF, EKF, and SEKF may have some limitations due to the approximations used to compute filter state transition and measurement matrices. PSELIKA, USKF, and DFEKF extend the capability of KF, EKF, and SEKF to tackle this issue as explained earlier in the introduction section. But USKF, and SEKF have a relatively higher computational load compared to KF, EKF, SEKF, and PSLEIKA. Fig. 1 shows a block diagram of the estimation algorithm presented in the current research article.

2.2.1. Extended Kalman Filter (EKF)

For systems that have nonlinearities in either the plant or the measurement processes, the EKF is used. The prediction of the state in the future is calculated using the Equation (8).

$$\hat{X}_k^{(-)} = f(\hat{X}_{k-1}) \quad (8)$$

where f is a nonlinear function that represents the system's behavior. In this case, f is calculated by combining (2) and (4), resulting in Equation (9).

$$f(X) = \begin{bmatrix} \frac{1}{2}\Xi Q_{I\to B} \\ J^{-1}[(J\omega + H_\omega)\times]\omega + J^{-1}(T_g + T_a + T_r + T_s) \end{bmatrix} \quad (9)$$

The a priori estimation error covariance is calculated using the Equation (10).

$$P_k^{(-)} = A_{k-1}P_{k-1}^{(+)}A_{k-1}^T + Q_{k-1} \quad (10)$$

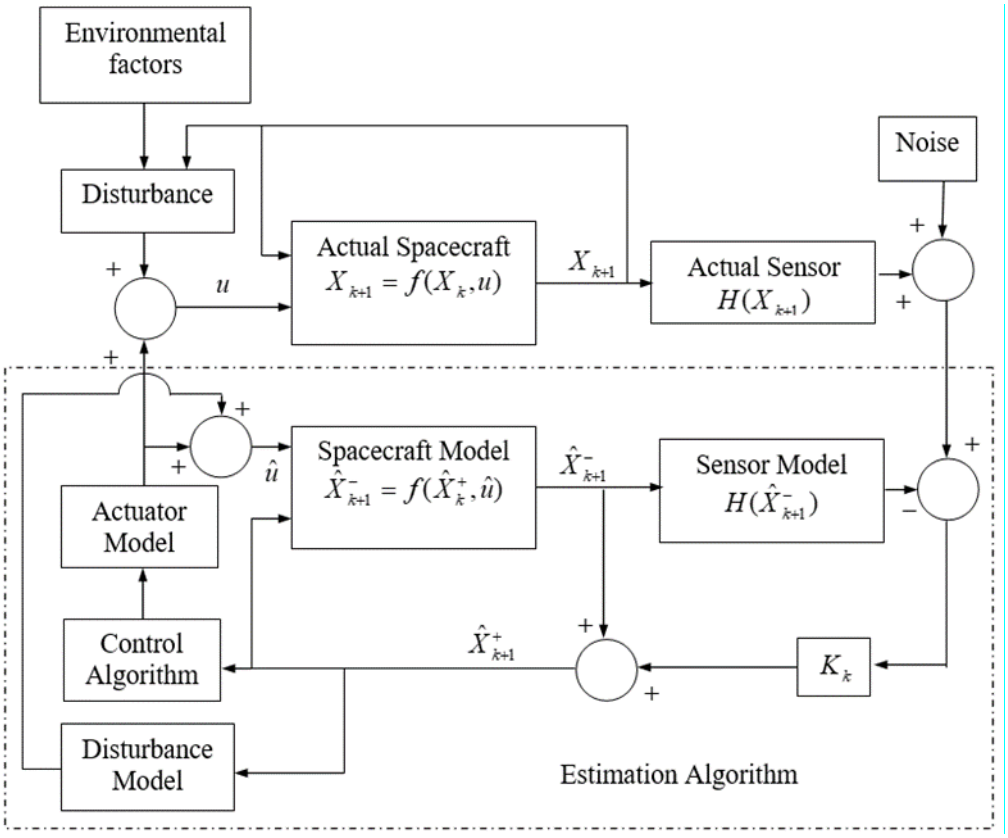

Fig. 1. Estimation algorithm block diagram

The measurement update stage is described by Equation (11) to (13).

$$K_k = P_k^{(-)} H_k^T \left(H_k P_k^{(-)} H_k^T + R_k \right)^{-1} \tag{11}$$

$$\hat{X}_k^{(+)} = \hat{X}_k^{(-)} + K_k [z_k - \hat{z}_k] \tag{12}$$

$$P_k^{(+)} = [I - K_k H_k] P_k^{(-)} [I - K_k H_k]^T + K_k R_k K_k^T \tag{13}$$

Where, $\hat{X}_k^{(+)}$ and, $P_k^{(+)}$ stand for the a posteriori state estimate and the error covariance, respectively. For numerical stability (13), uses the Joseph form of the estimation error covariance matrix. The state transition and measurement matrices can be calculated using the Equation (14) to (17).

$$A_{k-1}(\hat{X}_{k-1}^{(+)}) = \left\{ I + \left(F_{k-1}(\hat{X}_{k-1}^{(+)}) \right) \Delta T \right\} \tag{14}$$

$$F_{k-1}(\hat{X}_{k-1}^{(+)}) = \partial f / \partial X |_{(\hat{X}_{k-1}^{(+)})} \tag{15}$$

$$z_k = h_k(X_k) + v_k \tag{16}$$

$$H_k = \left. \frac{\partial h}{\partial X} \right|_{(\hat{X}_k^-)} \tag{17}$$

In the equations, ΔT represents the sampling period, and v_k is a zero-mean white Gaussian noise that is associated with the magnetometer measurements. The measurements used in this study are provided by a magnetometer, so the measurement vector, $h_k(X_k)$, is described as (18).

$$h_k(X_k) = B_B = D^{I \to B}(Q^{I \to B}) B_I \tag{18}$$

Where B_B represents the earth's magnetic field vector measured in the Body Coordinate System (BCS), and B_I represents the earth's magnetic field vector expressed in the Earth-Centered Inertial

(ECI) system. The transformation matrix from ECI to BCS, $D^{I\to B}$, can be calculated using the method described in (19) [27].

$$A(Q^{I\to B}) = \begin{bmatrix} q_1^2 - q_2^2 - q_3^2 + q_4^2 & 2(q_1q_2 + q_3q_4) & 2(q_1q_3 - q_2q_4) \\ 2(q_1q_2 - q_3q_4) & -q_1^2 + q_2^2 - q_3^2 + q_4^2 & 2(q_2q_3 + q_1q_4) \\ 2(q_1q_3 + q_2q_4) & 2(q_2q_3 - q_1q_4) & -q_1^2 - q_2^2 + q_3^2 + q_4^2 \end{bmatrix} \quad (19)$$

When considering the measurement noise covariance, it is important to note that its discrete form, represented by the matrix, R_k, is connected to its continuous form, represented by the matrix, $R(t)$, through the relation in Equation (20) [28].

$$R_k = R(t)/\Delta T \quad (20)$$

The matrix representing the process noise covariance in its discrete form, denoted by, Q_k, is related to its continuous form, denoted by, $Q(t)$, through the relation given in (21) [29].

$$Q_k = \int_0^{\Delta T} A(t_{k+1},\eta)Q\,A(t_{k+1},\eta)^T d\eta \quad (21)$$

It is also important to note that EKF has inherent an assumption which could represent a limitation. The first assumption is that Equation (14) assumes that the state transition matrix could be obtained using a Taylor series expansion till the first derivative ($\partial f/\partial X|$) only. Thus, a complete series expansion is very hard to obtain due to the mathematical complexity of the problem. In addition, the effect of disturbance forces and moments is very complex to be included in (14). Thus, Equation (14) and (17) are considered as approximate solutions.

2.2.2. Sequential Extended Kalman Filter (SEKF)

Sometimes, the EKF described in Section 2.2.1 is referred to as a batch EKF, because it processes all measurements at each time step as a batch. However, for embedded systems, this can present a challenge, as inverting a matrix of dimensions equal to the measurement noise covariance matrix, R_k, can be computationally intensive. To address this issue, the Sequential Extended Kalman Filter (SEKF) was introduced [30]. In SEKF, the measurement vector is divided into individual measurement elements, which are processed one by one through the relation in Equation (22).

$$Z_{i,k} = H_{i,k}X_k + v_{i,k} \quad (22)$$

Where, $Z_{i,k}$ is the measurement element number i ($i = 1, 2, \ldots\ldots, M$), and M is the length of the measurement vector. $H_{i,k}$ is the ith row of the measurement matrix, H_k. Equations for the SEKF filter are given as Equation (23) to (29).

$$\hat{X}_{0,k}^{(+)} = \hat{X}_k^{(-)} \quad (23)$$

$$P_{0,k}^{(+)} = P_k^{(-)} \quad (24)$$

$$K_{i,k} = P_{i-1,k}^{(-)}H_{i,k}^T\left(H_{i,k}P_{i-1,k}^{(+)}H_{i,k}^T + R_{i,k}\right)^{-1} \quad (25)$$

$$\hat{X}_{i,k}^{(+)} = \hat{X}_{i-1,k}^{(+)} + K_{i,k}\left[Z_{i,k} - \hat{Z}_{i,k}\right] \quad (26)$$

$$P_{i,k}^{(+)} = \left[I - K_{i,k}H_{i,k}\right]P_{i-1,k}^{(+)}\left[I - K_{i,k}H_{i,k}\right]^T + K_{i,k}R_{i,k}K_{i,k}^T \quad (27)$$

$$\hat{X}_k^{(+)} = \hat{X}_{M,k}^{(+)} \quad (28)$$

$$P_k^{(+)} = P_{M,k}^{(+)} \quad (29)$$

The SKF formulation assumes that the measurement matrix, R_k, is diagonal. In addition, the same assumption of the EKF applies to the SEKF also.

2.2.3. Pseudo Linear Kalman Filter (PSELIKA)

PSELIKA is similar to EKF in most contents of its structure. Instead of (8), the system is represented by Equation (30).

$$\hat{X}_k^{(-)} = f(\hat{X}_{k-1}) = \Lambda_{k-1}(\hat{X}_{k-1})\hat{X}_{k-1} + Bu \tag{30}$$

And the measurement process also is represented by Equation (31).

$$z_k(\hat{X}_k) = \Gamma_k(\hat{X}_k)\hat{X}_k + v \tag{31}$$

The remaining filter structure is the same as EKF but with replacing F_k, and H_k with Λ_k, and Γ_k respectively. The matrices Λ_k, and Γ_k could be computed as Equation (32) and (33).

$$B_B = \Gamma_k Q^{I \to B} \tag{32}$$

$$Q_m = \begin{bmatrix} q_4 & -q_3 & q_2 \\ q_3 & q_4 & -q_1 \\ -q_2 & q_1 & q_4 \\ -q_1 & -q_2 & -q_3 \end{bmatrix} \tag{33}$$

Where Γ_k is computed from Equation (34) to (36).

$$\Gamma_k = \begin{bmatrix} q_4 & -q_3 & q_2 \\ q_3 & q_4 & -q_1 \\ -q_2 & q_1 & q_4 \\ -q_1 & -q_2 & -q_3 \end{bmatrix} = Q_m^T E \tag{34}$$

and

$$E = \begin{bmatrix} [B_I \times] & B_I \\ -B_I^T & 0 \end{bmatrix} \tag{35}$$

$$\Lambda_{k-1} = \begin{bmatrix} 0_{4\times4} & 0.5Q_m \\ 0_{3\times4} & J^{-1}[(J\omega + H_w) \times] \end{bmatrix} \tag{36}$$

It is also important to note that the same assumption of the EKF also applies here. In addition, Equation (30) is a nonlinear equation shaped as a linear equation. This is because of that the matrix, Λ_{k-1}, is a function of the state vector. This makes the algorithm behaves like an ad-hoc algorithm.

2.2.4. Unscented Kalman Filter (USKF)

The USKF, or alternatively sigma point Kalman filter, propagates a number of points (sigma points) through system dynamics to relieve the problems encountered while computing the partial derivatives of the nonlinear differential equations describing the process and measurement models. First, (2N+1) points are generated (where N is the size of the state vector) according to the relations in Equation (37) and (38).

$$\gamma_{k-1}^0 = \hat{X}_{k-1} \tag{37}$$

$$[\Delta\gamma_1 \quad \cdots \quad \Delta\gamma_N] = \sqrt{(N+\kappa)P_{k-1}} \tag{38}$$

The tuning factor is preferred to be computed by the relation in Equation (39).

$$\kappa = 3 - N \tag{39}$$

Thus, N points are generated according to Equation (40).

$$\gamma_{I,k-1} = \hat{X}_{k-1} + \Delta\gamma_I \text{ and } I = 1,2,\ldots,N \tag{40}$$

And another N points are generated according to Equation (41).

$$\gamma_{N+I,k-1} = \hat{X}_{k-1} - \Delta\gamma_I \tag{41}$$

Now all of the generated (2N+1) points are projected a head of time through the relation in Equation (42).

$$\gamma_{J,k} = f(\gamma_{J,k-1}), \tag{42}$$

Where $J = 0,1,2,\ldots,2N$

A weighting strategy is accomplished by Equation (43) to (45).

$$W_J = \begin{cases} \dfrac{\kappa}{N+\kappa} & J = 0 \\ \dfrac{1}{2(N+\kappa)} & J = 1,2,\cdots 2N \end{cases}, \tag{43}$$

Where $J = 0,1,2,\ldots,2N$

$$\hat{X}_k^- = \sum_{J=0}^{2N} W_J \gamma_{J,k} \tag{44}$$

$$P_k^- = \sum_{J=0}^{2N} W_J (\gamma_{J,k} - \hat{X}_k^-)(\gamma_{J,k} - \hat{X}_k^-)^T + Q_k \tag{45}$$

A set of measurement could be generated and weighted at each point using the relation in Equation (46) and (47).

$$Z_{J,k} = h(\gamma_{J,k}) \tag{46}$$

$$\hat{z}_k = \sum_{J=0}^{2N} W_J \, Z_{J,k} \tag{47}$$

Now the state of the system could be updated after obtaining the measurements via the relations in Equations (48) to (52).

$$P_{zz} = \sum_{J=0}^{2N} W_J (Z_{J,k} - \hat{z}_k)(Z_{J,k} - \hat{z}_k)^T + R_k \tag{48}$$

$$P_{xz} = \sum_{J=0}^{2N} W_J (\gamma_{J,k} - \hat{X}_k^-)(Z_{J,k} - \hat{z}_k)^T \tag{49}$$

$$K_k = P_{xz}(P_{zz})^{-1} \tag{50}$$

$$\hat{X}_k^{(+)} = \hat{X}_k^{(-)} + K_k[z_k - \hat{z}_k] \tag{51}$$

$$P_k = P_{xx} - K_k P_{zz} K_k^T \tag{52}$$

It is now important to mention that the USKF reliefs all the assumptions of the EKF, SEKF, and PSELIKA filters. This extends the algorithm capability to very complex mathematical modelling due to the elimination of the need to calculate the partial derivatives which in many cases becomes impossible.

2.2.5. Derivative Free Extended Kalman Filter (DFEKF)

DFEKF is very similar to USKF. It begins with generating (N+1) sigma points according to the relations in Equation (53) and (54).

$$[\Delta\gamma_1 \quad \cdots \quad \Delta\gamma_N] = \sqrt{NP_{k-1}} \tag{53}$$

$$\gamma_{I,k-1} = \hat{X}_{k-1} + \frac{1}{\beta}\Delta\gamma_I, \text{ and } I = 1,2,\ldots,N \tag{54}$$

The (N+1) points could now be propagated through the relations in Equation (55) and (56).

$$\hat{X}_k^{(-)} = f\left(\hat{X}_{k-1}\right) \tag{55}$$

$$\gamma_{J,k} = f\left(\gamma_{J,k-1}\right), \tag{56}$$

Where $J = 0,1,2,\ldots,2N$.

With estimation error covariance matrix given by (57) to (59).

$$P_k^{(-)} = \frac{\beta}{N}\sum_{I=1}^{N}\left(\gamma_{I,k} - \hat{X}_k^{(-)}\right)\left(\gamma_{I,k} - \hat{X}_k^{(-)}\right)^T + Q_k, \tag{57}$$

Where $J = 0,1,2,\ldots,2N$.

$$\Delta y_I = [\Delta y_1 \quad \Delta y_2 \quad \cdots \quad \Delta y_N]^T = \sqrt{NP_k^{(-)}} \tag{58}$$

$$y_{I,k} = \hat{X}_k^{(-)} + \frac{1}{\beta}\Delta y_I \tag{59}$$

For the DFEF to perform like EKF, the tunable constant, β, could be chosen large. A set of measurements are generated according to Equation (60) and (61).

$$Z_{I,k} = h\left(y_{I,k}\right) \tag{60}$$

$$\hat{z}_k = h\left(\hat{X}_k^{(-)}\right) \tag{61}$$

With measurement update given by Equations (62) to (66).

$$P_{xz} = \frac{\beta}{N}\sum_{I=1}^{N}\left(\gamma_{I,k} - \hat{X}_k^{(-)}\right)\left(Z_{I,k} - \hat{z}_k\right)^T \tag{62}$$

$$P_{zz} = \frac{\beta}{N}\sum_{I=1}^{N}\left(Z_{I,k} - \hat{z}_k\right)\left(Z_{I,k} - \hat{z}_k\right)^T + R_k \tag{63}$$

$$K_k = P_{xz}(P_{zz})^{-1} \tag{64}$$

$$\hat{X}_k^{(+)} = \hat{X}_k^{(-)} + K_k[z_k - \hat{z}_k] \tag{65}$$

$$P_k = P_{xx} - K_k P_{xz}^T \tag{66}$$

It is also important to mention that the DEFEK belongs to the same family of the USKF. Thus, the inherent assumptions of EKF, SEKF, and PSELIKA, are also relieved. This enhances also capability of the algorithm to deal with any nonlinear and mathematically complex problems.

2.2.6. Observability

Floquet theory can be used to ensure that the discrete filter system is observable by calculating the relationship in Equation (67) [7],

$$\Theta = \prod_{k=1}^{N}[I - K_{k+1}H_{k+1}]A_{k+1} \tag{67}$$

For the estimator to be stable, all the eigenvalues of the matrix, Θ, should have a magnitude smaller than one in the steady-state region of the filter. The maximum eigenvalue being small indicates the rate of convergence.

3. Results and Discussion

The proposed estimation algorithms are compared to an EKF, and SEKF algorithms which were verified in [2][17]. The verification process in [2][17] was based on verified simulators of the former Egyptian Spacecraft EGYPTSAT-1, launched in April 2007. The spacecraft has an orbit inclination angle of 98.085°, semi-major axis of 7039200 m, eccentricity of 0, true anomaly angle of 0°, a right ascension of ascending node of 337.5°, and argument of perigee angle of 69°. The epoch time is 17th April 2007 at 00:00:00. The spacecraft's initial attitude angles are 85°, 170°, and -165° for pitch, roll, and yaw respectively. The initial attitude angular rates are -0.2°/s, 0.8°/s, and 0.7°/s for pitch, roll, and yaw respectively. All of the proposed estimation algorithms in addition to the EKF, and SEKF have initial conditions that are all zero. This means there is no initial attitude information, which is the case for detumbling conditions after separation from the launcher. The spacecraft's inertial characteristics are J_x=11.2 Kg.m^2, J_y=11.4 Kg.m^2, J_z=9.2 Kg.m^2, J_{xy}=0.02 Kg.m^2, J_{xz}=-0.08 Kg.m^2, and J_{yz}=0.2 Kg.m^2. A simulation time step of 4 seconds is utilized. The standard deviation of the magnetometer error is 200 nT for each axis of the three magnetometer axes. The largest allowable deviation from the intended angle is ±7° when using low accuracy operation modes and ±0.5° when using high accuracy operation modes. The developed algorithms in the current study for the PSELIKA, USKF, and DFEKF are compared to the previously verified studies for the SEKF [2], and EKF [17].

Measurements of a three-axis magnetometer are being used. Fig. 2 shows the history of time for the attitude estimation error, while Fig. 3 displays the estimation error of the vector components of the angular velocity. As illustrated in Fig. 2 and Fig. 3, the filter achieves steady state performance quickly after only 0.4 orbits. The EKF, and SEKF in addition to all of the suggested algorithms can reach convergence, even when encountering significant initial attitude estimation errors commonly experienced in the detumbling mode. Therefore, these algorithms can be applied during any operational mode of the spacecraft, regardless of whether it is a high accuracy or low accuracy mode. Computations were performed using a personal computer equipped with a Core (TM) i7 CPU with a processing speed of 2.6 GHz and 8 GB of RAM. The MATLAB R2022b environment was used for the calculations.

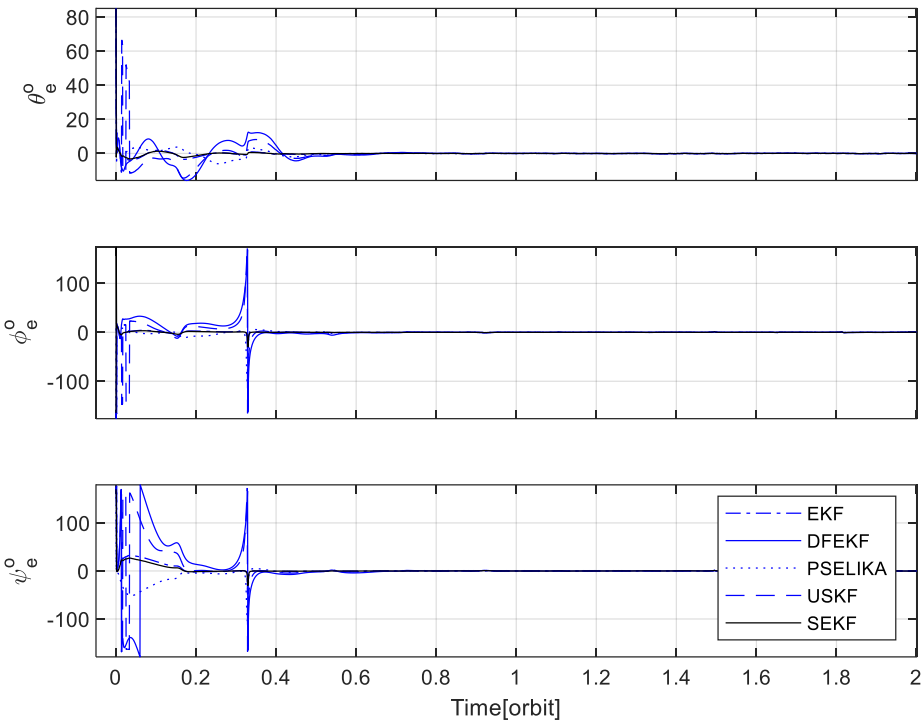

Fig. 2. Time history of spacecraft attitude estimation error for different filters

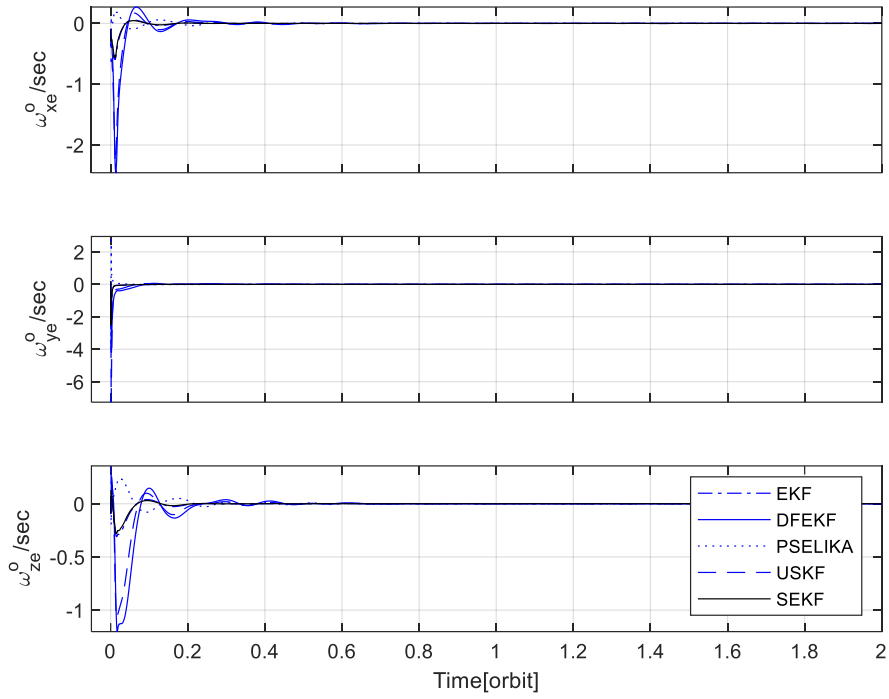

Fig. 3. Time history of spacecraft angular velocity estimation error for different filters

Table 1 displays the execution time of the developed estimation algorithms and their corresponding accuracies. As shown in Table 1, PSELIKA has the lowest estimation errors and execution time and the least maximum eigenvalue. Thus, its performance is considered as the best performance because it has the best key performance indices. As depicted also in Table 1, The EKF, and SEKF have nearly the same accuracy levels. DFEKF has an accuracy level better than EKF, and SEKF because it doesn't depend on computing a state transition matrix. This could be done through the propagation of (N+1) sigma points. The USKF has an accuracy better than EKF, SEKF, and DFEKF because it uses the propagation of (2N+1) sigma points. This results in a more execution time and higher accuracy levels. The standard deviations of the estimation errors for all of the estimation algorithms have a very low error standard deviation (which are below the value of 0.15) compared to the maximum permitted angular error (which is ± 7 degrees when using low accuracy operation modes and ± 0.5 degrees when using high accuracy operation modes) despite the fact that the magnetometer has very large measurement error compared to the cited articles (which use normally a magnetometer standard deviation of 50 nT, or a maximum of 100 nT). According to the obtained accuracy levels, the magnetometer could be used solely to provide all the required attitude information in all of the spacecraft operational mode without the need to any other sensor.

Table 1. Key performance indices for different filters

	Yaw angle error standard deviation (deg.)	Pitch angle error standard deviation (deg.)	Roll angle error standard deviation (deg.)	Maximum Eigen Value at the end of simulation time	Average Execution time (s)
EKF	0.14	0.0548	0.131	$9.8\text{x}10^{-6}$	0.0541
DFEKF	0.1283	0.0551	0.1283	0.3297	0.0584
PSELIKA	0.0143	0.0034	0.0154	$1.3131\text{x}10^{-7}$	0.0536
USKF	0.0547	0.0549	0.1361	0.9372	0.0715
SEKF	0.1402	0.0547	0.131	0.2288	0.0538

Time history of the processor execution time can be seen in Fig. 4. It is clear that, on average, SEKF requires less execution time when compared to EKF. Specifically, on the aforementioned hardware configuration, the average execution time of the SEKF algorithm is 0.0538 seconds.

Additionally, in a separate study [30], a filter named the $\alpha\beta$ filter was proposed and compared to EKF. The execution times for the EKF and $\alpha\beta$ filters on a personal computer (PC) were measured to be 0.74 and 0.39 seconds, respectively. By comparing these values to the execution time of the developed SEKF algorithm in the current research (which is 0.0537 seconds), we can see the significant improvement in performance of the SEKF algorithm. It is important to note that the hardware and software configurations between the current research and the previous study in [30] are different, but the results clearly indicate the superior performance of the developed SEKF algorithm. Furthermore, all of the developed algorithms in this research does not rely on small angles approximations. Therefore, they are capable of handling large initial attitude estimation errors and still converge. The graph in Fig. 5 displays the change in the magnitude of the maximum eigenvalue of the matrix, Θ, over time. As depicted in the graph, the magnitude of the maximum eigenvalue of the matrix, Θ, becomes less than one after one orbital period and continues to decrease as time elapses. This indicates that the estimator is converging at a faster rate, leading to improved performance.

Based on the results obtained, the accuracy level obtained in the current manuscript is about 0.14^{o} in the worst case which is much better than the typical value of 0.5^{o}. Thus, the developed algorithms could utilize magnetometer as a sole spacecraft attitude sensor and provide the spacecraft with the prescribed accuracy levels. This in turn:

1- Eliminates the need for other expensive, heavy, complex, and electric power consuming sensors which are usually utilized to provide such accuracy level.

2- Minimizes the spacecraft electrical power requirements.

3- Minimizes excessive weight and cost of sensors.

4- Minimizes the weight of the spacecraft power subsystem.

5- Increases the accuracy of the AOCS.

6- Increases the life time and reliability of the spacecraft due to the absence of complicated sensors

7- Reduces total spacecraft weight which means a reduction in the spacecraft launch cost.

8- Enhances the ability of the spacecraft to execute any required attitude maneuver in space.

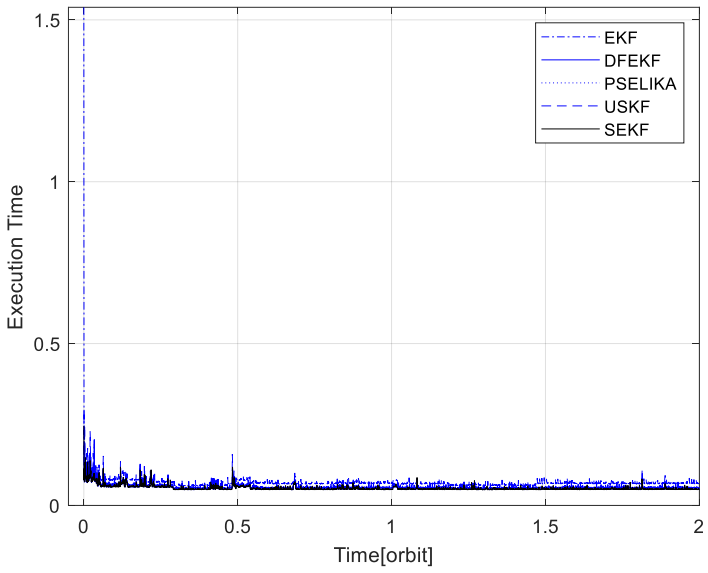

Fig. 4. Execution time for different filters

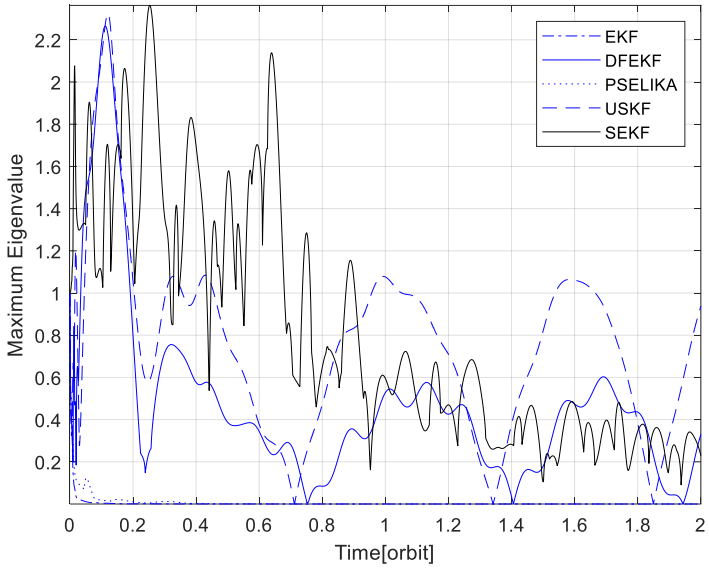

Fig. 5. Maximum eigenvalue time history for different filters

Thus, the current study provided better accuracy levels as depicted in Table 1 for the PSLEIKA, USKF, and DFEKF compared to (SEKF) developed in [2], and EKF developed in [17]. The superior performance metrics obtained by PSLEIKA makes it an attractive solution for the problem at hand in terms of its accuracy, and execution tome on-board the spacecraft compared to USKF, and DFEKF.

4. Conclusion

Algorithms for estimating the angles and angular velocities of a spacecraft are developed using only measurements from a three-axis magnetometer based on PSELIKA, USKF, and DFEKF. These algorithms are based on KF formulation and have been compared to an EKF, and SEKF. The developed algorithms can provide an attitude accuracy of at least 0.14º or better in each axis. This accuracy level means that the algorithm can be used without the need for additional sensors, reducing the overall cost of the spacecraft mission while still maintaining the same level of accuracy, higher reliability, and lifespan. The need for additional Attitude and Orbit Control System (AOCS) devices, such as star sensors or gyroscopes, is eliminated due to the high accuracy levels obtained. The developed algorithms don't assume small angle approximations. Quaternion vectors are used to represent the spacecraft's attitude because they don't experience singularity problems at large attitude angles. As a result, the algorithms can still converge even with very large initial attitude estimation errors of 85 degrees, 170 degrees, and -165 degrees for pitch, roll, and yaw respectively. Convergence is achieved with high accuracy levels much better than 0.5º. The achieved accuracy (which is much better than0.5º), execution time (which is 0.0715s in the worst case), and convergence capabilities allow the proposed algorithms to function in all operational modes of the spacecraft. Observability and convergence rates of the presented algorithms have been assessed using Floquet theory, and the maximum obtained eigenvalue of matrix, Θ, have a magnitude smaller than one after only one orbit. This indicates a good convergence rate and stability for the estimators. The best estimation error performance is achieved by PSELIKA in terms of all of the performance measures.

The author plans to conduct further research by implementing the newly developed algorithms within a hardware-in-the-loop simulator (HIL). Following successful testing within HIL, the next step will involve deploying the algorithms as reserve options for a real spacecraft mission which is currently under development by the National Authority for Remote Sensing and Space Sciences (NARSS). Once the effectiveness of the reserve algorithms has been validated, the developed algorithms could be used as a standalone system for the mission. In addition, the developed algorithms in the current research article could be used to provide training data set. Thus, they will be combined

with AI algorithms presented in Refs [19]-[26] to provide an integrated solution for the spacecraft AOCS.

Author Contribution: This paper has a single author who contributed to this paper, and approved the final version.

Funding: The Author declares that this work is supported by the National Authority for Remote Sensing and Space Sciences (NARSS) under project code 0725/SR/SPA/2022. MATLAB license is provided by Nile University. The APC is funded by International Journal of Robotics and Control Systems.

Acknowledgment: Language editing service is provided by ChatGPT.

Conflicts of Interest: The authors declare no conflict of interest.

References

[1] R. Kalman, "A New Approach for Linear Filtering and Prediction Problems," *Transactions of the ASME–Journal of Basic Engineering*, vol. 82, pp. 35–45, 1960, https://doi.org/10.1115/1.3662552.

[2] T. M. A. Habib, "Three-axis High-Accuracy Spacecraft Attitude Estimation via Sequential Extended Kalman Filtering of Single-Axis Magnetometer Measurements," *Aerospace Systems*, pp. 1-10, 2023, https://doi.org/10.1007/s42401-023-00221-w.

[3] D. Simon, *Optimal State Estimation, Kalman, H_{∞}, and Nonlinear Approaches*. John Wiley and Sons, 2006, https://doi.org/10.1002/0470045345.

[4] T. M. Habib, "In-Orbit Spacecraft Inertia, Attitude, and Orbit Estimation Based on Measurements of Magnetometer, Gyro, Star Sensor and GPS Through Extended Kalman Filter," *International Review of Aerospace Engineering (IREASE)*, vol. 11, no. 6, pp. 247-251, 2018, https://doi.org/10.15866/irease.v11i6.14839.

[5] D. C. Guler, E. S. Conguroglu, and C. Hajiyev, "Single-Frame Attitude Determination Methods for Nano-Satellites," *Metrology and Measurement Systems*, vol. 24, no. 2, pp. 313–324, 2017, https://journals.pan.pl/Content/107372/PDF/139.pdf.

[6] J. K. Deutschmann, and I. Y. Bar-Itzhack, "Evaluation of Attitude and Orbit Estimation Using Actual Earth Magnetic Field Data," *Journal of Guidance Control and Dynamics*, vol. 24, no. 3, pp. 616–623, 2001, https://doi.org/10.1002/0470045345.

[7] M. L. Psiaki, F. Martel, and P. K. Pal, "Three-Axis Attitude Determination via Kalman Filtering of Magnetometer Data," *Journal of Guidance Control and Dynamics*, vol. 13, no. 3, pp. 506–514, 1990, https://doi.org/10.2514/3.25364.

[8] F. L. Markley and D. Mortari "Quaternion Attitude Estimation using Vector Observations," *Journal of the Astronautical Sciences*, vol. 48, no. 2, pp. 359–380, 2000, https://doi.org/10.1007/BF03546284.

[9] T. Habib, "Spacecraft Attitude and Orbit Determination from the Cost and Reliability Viewpoint: A Review," *ASRIC Journal on Natural Sciences*, vol. 1, pp. 14–35, 2022, https://asric.africa/documents/Journal/journal%202022%20-%20natural%20sciences%20-%20v1.pdf.

[10] C. Hajiyev and D. C. Guler, "Attitude and Gyro Bias Estimation by SVD-aided EKF," *Measurement*, vol. 205, 2022, https://doi.org/10.016/j.measurement.2022.112209.

[11] C. Hajiyev and D. C. Guler, "Review on Gyroless Attitude Determination Methods for Small Satellites," *Progress in Aerospace Sciences*, vol. 90, pp. 54–66, 2016, https://doi.org/10.1016/j.paerosci.2017.03.003.

[12] T. Bak, *Spacecraft Attitude Determination- a Magnetometer Approach*. Aalborg University, 1999, https://vbn.aau.dk/en/publications/spacecraft-attitude-determination-a-magnetometer-approach.

[13] S. Carletta, P. Teofilatto, and M. S. Farissi, "A Magnetometer-Only Attitude Determination Strategy for Small Satellites: Design of the Algorithm and Hardware-in-the-Loop Testing," *Aerospace*, vol. 7, no. 1, p. 3, 2020, https://doi.org/10.3390/aerospace7010003.

[14] C. Hart, "Satellite Attitude Determination Using Magnetometer Data Only," *47th AIAA Aerospace Sciences Meeting Including The New Horizons Forum and Aerospace Exposition*, p. 220, 2009, https://doi.org/10.2514/6.2009-220.

[15] K. Han, H. Wang, and Z. Jin, "Magnetometer-Only Linear Attitude Estimation for Bias Momentum Pico-Satellite," *Journal of Zhejiang University-SCIENCE A*, vol. 11, no. 6, pp. 455–464, 2010, https://doi.org/10.1631/jzus.A0900725.

[16] G. -F. Ma and X. -Y. Jiang, "Unscented Kalman Filter for Spacecraft Attitude Estimation and Calibration Using Magnetometer Measurements," *2005 International Conference on Machine Learning and Cybernetics*, pp. 506-511, 2005, https://doi.org/10.1109/ICMLC.2005.1526998.

[17] T. M. A. Habib, "A Comparative Study of Spacecraft Attitude Determination and Estimation Algorithms (A cost-benefit approach)," *Aerospace Science and Technology*, vol. 26, no. 1, pp. 211–215, 2013, http://dx.doi.org/10.1016/j.ast.2012.04.005.

[18] T. M. A. Habib, "Artificial Intelligence for Spacecraft Guidance, Navigation, and Control: A state-of-the-art," *Aerospace Systems*, vol. 5, pp. 503–521, 2022, https://doi.org/10.1007/s42401-022-00152-y.

[19] T. M. A. Habib, "Spacecraft Nonlinear Attitude Dynamics Control with Adaptive Neuro-Fuzzy Inference System," *International Review of Automatic Control*, vol. 12, no. 5, pp. 242–250, 2019, https://doi.org/10.15866/ireaco.v12i5.18056.

[20] T. M. A. Habib, "Nonlinear Spacecraft Attitude Control via Cascade-Forward Neural Networks," *International Review of Automatic Control*, vol. 13, no. 3, pp. 146–152, 2020, https://doi.org/10.15866/ireaco.v13i3.19149.

[21] T. M. A. Habib and R. A. Abouhogail, "In-Orbit Three-Axis Spacecraft Orbit Control Based on Neural Networks via Limited Thrust Budget," *International Review of Automatic Control*, vol. 14, no. 3, pp. 144–152, 2021. https://doi.org/10.15866/ireaco.v14i3.20262.

[22] T. M. A. Habib, "Replacement of In-Orbit Modern Spacecraft Attitude Determination and Estimation Algorithms with Neural Networks," *International Review of Aerospace Engineering*, vol. 14, no. 3, pp. 166–172, 2021, https://doi.org/10.15866/irease.v14i3.19687.

[23] T. M. A. Habib, "Replacement of In-Orbit Extended Kalman Filter for Spacecraft Orbit Estimation via Neural Networks," *International Review of Automatic Control*, vol. 14, no. 4, pp. 224–232, 2021, https://doi.org/10.15866/ireaco.v14i4.20948.

[24] T. M. A. Habib and R. A. Abouhogail, "Replacement of In-Orbit Spacecraft Attitude Determination Algorithms with Adaptive Neuro-Fuzzy Inference System via Subtractive Clustering," *International Review of Aerospace Engineering*, vol. 14, no. 4, pp. 220–227, 2021, https://doi.org/10.15866/irease.v14i4.20020.

[25] T. M. A. Habib and R. A. Abouhogail, "Modelling of Spacecraft Orbit via Neural Networks," *International Review of Aerospace Engineering*, vol. 14, no. 5, pp. 285–293, 2021, https://doi.org/10.15866/irease.v14i5.20083.

[26] T. M. A. Habib and R. A. Abouhogail, "Efficient Simultaneous Spacecraft Attitude and Orbit Estimation via Neural Networks," *International Review of Aerospace Engineering*, vol. 14, no. 6, pp. 346–353, 2021, https://doi.org/10.15866/irease.v14i6.20312.

[27] M. J. Sidi, "Spacecraft Dynamics and Control, a Practical Engineering Approach," *Cambridge University Press*, vol. 7, 1997, https://doi.org/10.1017/CBO9780511815652.

[28] R. G. Brown and P. Hwang, "Introduction to Random Signals and Applied Kalman Filtering," *John Wiley and Sons Inc.*, 1997, https://books.google.co.id/books?id=6f5SAAAAMAAJ.

[29] A. Smyth and M. Wu, "Multi-rate Kalman filtering for the data fusion of displacement and acceleration response measurements in dynamic system monitoring," *Mechanical Systems and Signal Processing*, vol. 21, no. 2, pp. 706–723, 2007, https://doi.org/10.1016/j.ymssp.2006.03.005.

[30] H. Boussadia, M. A. S. Mohammed, N. Boughanmi, A. Meche, and A. Bellar, "A Combined Configuration (αβ filter- TRIAD algorithm) for Spacecraft Attitude Estimation based on in-Orbit Flight Data," *Aerospace systems*, vol. 5, pp. 223–232, 2022, https://doi.org/10.1007/s42401-021-00115-9.